Time-resolved anomalous small angle X-ray scattering at BL28XU

Small angle X-ray scattering has been widely used in the characterization of colloids, gels, metals, polymers and proteins on a length scale from just above atomic size up to several 100 nanometers. Anomalous small angle X-ray scattering (ASAXS) is a contrast variation scattering technique that enables us to estimate the partial structure factors in a multi-component system [1,2]. In the ASAXS experiment, we measured the change in the scattered intensity with incident X-ray energy near the absorption edges of one component in the multi-component system. Near absorption edges, the scattering length or contrast factor of X-ray for scattering drastically changes. The analyses of the scattered intensity variation with the incident X-ray energy yielded each partial structure factor of the multi-component system. However, in the previous ASAXS experiments, it was difficult to conduct the time-resolved ASAXS measurement quickly since it took several ten seconds to adjust the X-ray energy of the incident beam. Thus, we constructed the anomalous ultra-small-angle X-ray scattering (AUSAXS) system at SPring-8 **BL28XU** for a time-resolved AUSAXS experiment [3]. At BL28XU, we can quickly adjust the energy of the incident X-ray without drifting the beam position [4], and conduct the time-resolved AUSAXS measurement. We also extended the path length to 9.1 m and attained the minimum $q = 0.0069$ nm^{-1} at 9 KeV.

Figure 1 shows a schematic illustration of the AUSAXS equipment for BL28XU. This beamline consists of optics hutch, experimental hutch 1, and experimental hutch 2. The optical setup includes the first mirror (M1), second mirror (M2), a monochromator (MONO), two jaw slits (SLIT1 and SLIT2) in the optics hutch, and third mirror (M3), fourth mirror (M4) and the other two jaw slits (SLIT3 and SLIT4) in the experimental hutch 1. The details of each component are described in the previous paper (Tanida *et al.* [4]). The setup enables us to change the energy of the X-ray with the beam position at the focal point being virtually constant. In addition to the existing optical setup, we installed the new components for the AUSAXS setup, consisting of the attenuator box, the scatterless slit, and the guard slit, as shown in Fig. 1.

The sample changer can be replaced with the heater block, which allows a sample to be heated up to 200°C, and the tensile machine for *in situ* observations during heating and stretching processes of samples. The ion chamber is mounted behind the sample to measure the transmittance of the samples. All components, including the glove box and the following polyvinyl chloride (PVC) flight paths, are evacuated to reduce parasitic scattering, as schematically shown at the bottom of Fig. 1. As a result, the AUSAXS system was completed with a sample-to-detector distance of 9.1 m. The beam stopper was a tungsten rod with

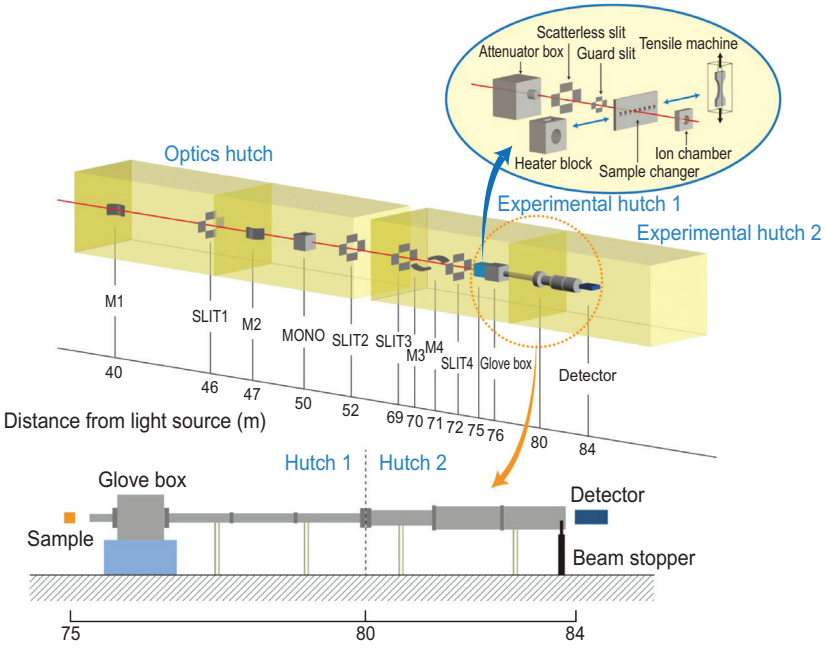

Fig. 1. A schematic illustration of the BL28XU beamline.

a width of 2 mm and an optical axis length of 4 mm. The USAXS/AUSAXS profiles were obtained with a two-dimensional hybrid pixel array detector, PILATUS 300K-W.

To check the availability of time-resolved AUSAXS, we observed the change of zinc oxide (ZnO) structures with time during the vulcanization of rubber. It is well-known that the addition of ZnO in rubber accelerates the vulcanization with sulfur and that the spatial distribution of ZnO affects the physical properties of vulcanized rubbers. By applying time-resolved AUSAXS near zinc *K*-edge to the vulcanization of rubber, we can extract the information on the change in the structures of ZnO during the vulcanization. We used poly(styrene-*ran*-butadiene) (SBR) as rubber.

We measured the scattering profiles at the following 17 different energies in one cycle with 30 s. The scattered intensity varied with the energy of X-ray. $I(q,E)$ is, thus, expressed by

$$I(q,E) = (\mu/A)^2 \left[f_0^2 F_0^2(q) + 2 f_0 f'(E) F_0(q) \nu(q) + (f'^2(E) + f''^2(E)) \nu^2(q) \right] \quad (1)$$

where f_0, A, μ, $f'(E)$, $f''(E)$, $F_0(q)$ and $\nu(q)$ are, respectively, the atomic scattering factor, molar mass, specific gravity, real parts of anomalous dispersion, imaginary parts of anomalous dispersion, the non-resonant and resonant amplitudes. We estimated $\nu^2(q)$ from the scattered intensity below the *K*-edge of Zn. Figure 2 shows the change in $\nu^2(q)$ with t. We found the shoulder at q = 0.01 nm^{-1} in $\nu^2(q)$, indicating that the clusters of ZnO with their size being about 100 nm in the system. We fitted $\nu^2(q)$ with the following the Unified Guinier/power-law equation:

$$\nu^2(q) = \nu^2(0)\, exp(-R_g^2/3) + Bq^{-p} \quad (2)$$

where $\nu^2(0)$, R_g, B and p are, respectively, $\nu^2(q)$ at $q = 0$, the radius of gyration of ZnO clusters, the prefactor of the power-law and the exponent of the power-law. The equation can be well fitted with the experimental results and the fitting results yielded the characteristic parameters. We listed them in Table 1. The size of particles of ZnO and the exponent decrease with time associating with the progress of the vulcanization.

We succeeded in constructing the AUSAXS measurement system by taking advantage of SPring-8 BL28XU beamline. The *q*-range for the AUSAXS measurement system was estimated to be 0.0069–0.3 nm^{-1}. We can obtain the scattering profiles at the 17 different X-ray energies in 30 s and conduct time-resolved measurements to investigate the changes in the structure of zinc compounds in SBR rubber during vulcanization. The change in the energy dependence of $I(q,E)$ with time was found during vulcanization, suggesting the transformation of zinc by the vulcanization reaction.

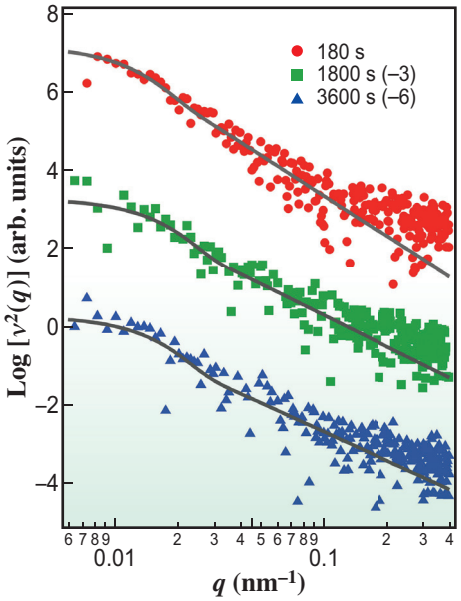

Fig. 2. The change in $\nu^2(q)$ with time plotted as a function of q. The amount of shift of the plots is shown in the legend.

Since we can conduct time-resolved AUSAXS measurement with the system, we can investigate the kinetics of the element-specific structure in the order of submicron scale. Thus we can apply the system to the basic research on the association processes of metal ion in gelation and phase separation dynamics of metal alloys, and the industrial materials including metals.

Table 1. Characteristic parameters obtained by fitting Eq. (2)

Time (s)	ν^2 (0)	R_g (nm)	B	p
180	1.50×10^{7}	1.7×10^{2}	8.1×10^{-1}	3.4
1800	2.0×10^{6}	1.3×10^{2}	4.30	2.7
3600	1.9×10^{6}	1.4×10^{2}	7.1	2.4

Mikihito Takenaka

Institute for Chemical Research, Kyoto University

Email: takenaka@scl.kyoto-u.ac.jp

References

[1] O. Lyon and J. P. Simon: Phys. Rev. B Condens. Matter. **35** (1987) 5164.
[2] Y. Watanabe *et al.*: J. Appl. Crystallogr. **56** (2023) 461.
[3] *Y. Nakanishi, S. Fujinami, M. Shibata, T. Miyazaki, K. Yamamoto and M. Takenaka.: J. Appl. Crystallogr. **57** (2024) 215.*
[4] H. Tanida *et al.*: J. Synchrotron Rad. **21** (2013) 268.